Numerical Modeling of Passive Scalar Transport in Shallow Water Based on the Quasi-Gasdynamic Approach

T. G. Elizarova[a],* and A. V. Ivanov[a],**

[a] *Federal Research Center Keldysh Institute of Applied Mathematics, Russian Academy of Sciences, Moscow, 125047 Russia*

*e-mail: telizar@mail.ru

**e-mail: alexvladiv@mail.ru

Abstract—A new method for the numerical solution of the passive scalar transport equation in the framework of hydrodynamic equations in the shallow water approximation is described. The method is based on previously developed quasi-gasdynamic algorithms for numerical simulation of compressible gas flows. Smoothed equations are derived, and their difference approximations, including for flows with a pollutant source, are presented. The numerical algorithms are tested as applied to one- and two-dimensional flows. As an example, the algorithm is used to solve the problem of water circulation in Lake Vallunden. The constructed approach is generalized to passive scalar transport in the case of viscous incompressible flows.

Keywords: shallow water equations, pollutant transport, regularized equations, finite volume method, source term, Lake Vallunden

DOI: 10.1134/S0965542520070064

1. INTRODUCTION

Simulation of passive scalar transport in the framework of hydrodynamic equations is widely used in applications, where the scalar can be regarded as pollutant, salinity, or temperature. We consider fluid dynamics equations in the shallow water (SW) approximation with allowance for passive scalar transport. Let the passive scalar concentration be denoted by C. In this case, the mathematical model consists of the SW equations

$$\frac{\partial h}{\partial t} + \text{div}\,(h\mathbf{u}) = 0, \tag{1}$$

$$\frac{\partial (h\mathbf{u})}{\partial t} + \text{div}\,(h\mathbf{u} \otimes \mathbf{u}) + \nabla \frac{gh^2}{2} = h(\mathbf{f} - g\nabla b), \tag{2}$$

which are supplemented with the passive scalar transport equation. The latter can be written in two versions:

$$\frac{\partial Ch}{\partial t} + \text{div}\,(\mathbf{u}Ch) = \text{div}\,(Dh\nabla C), \tag{3}$$

$$\frac{\partial C}{\partial t} + \text{div}\,(\mathbf{u}C) = \text{div}\,(D\nabla C). \tag{4}$$

The notation is explained in Fig. 1; here, $h(\mathbf{x}, t)$ is the water layer thickness measured from the bottom; $b(\mathbf{x})$ is the bottom topography; $\mathbf{u}(\mathbf{x}, t)$ is the vector of horizontal velocities; g is the acceleration of gravity, which is aligned with the z axis; $\mathbf{f}(\mathbf{x}, t)$ is a body force acting throughout the fluid depth, for example, the Coriolis force; $C(\mathbf{x}, t)$ is a passive scalar, which can be the pollutant concentration, salinity, or temperature (in what follows, without loss of generality, $C(\mathbf{x}, t)$ is understood as the pollutant concentration); D is the diffusion coefficient of the pollutant; and $\xi(\mathbf{x}, t) = h(\mathbf{x}, t) + b(\mathbf{x})$ is the water surface elevation.
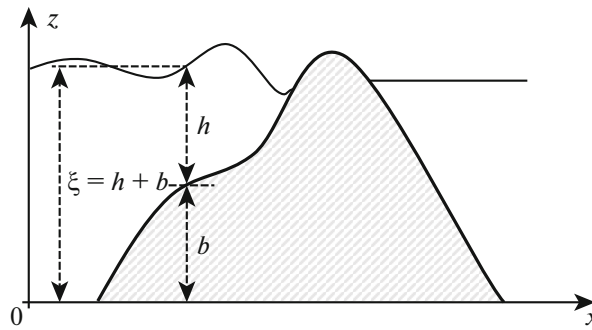
Fig. 1. Schematic explanation of the used notation.

The passive scalar transport equation given by (3) is often used in hydrological problems and allows for the "live" flow section, i.e., the cross-sectional area of the flow perpendicular to the direction of the velocity.

Equation (4) is a classical transport equation, where the pollutant is assumed to be passive and does not interact with the flow. However, in certain cases, other phenomena, such as pollutant sedimentation, sources, sinks, and erosion have to be taken into account; these phenomena are not considered in the presented equations.

Since an equation of the form (3) is most frequently used in practical computations, in what follows, talking about passive scalar transport in shallow water, we mean system (1)−(3).

The development of an efficient and accurate numerical algorithm for solving system (1)−(3) is a complicated task. Primarily, this is caused by the fact that solutions of this system are generally not smooth: they may contain hydrodynamic discontinuities and rarefaction waves for Eqs. (1) and (2) and discontinuities in the solution of transport equation (3). Additionally, a frequent situation in problems is that the diffusion coefficient D is very low. As a result, a number of schemes for the numerical solution of the transport equation turn out to be unstable or excessively dissipative, which complicates the numerical simulation and necessitates the development of methods for solving this problem. A possible approach is to apply a special separate algorithm for solving the transport equation, but this makes the numerical solution of system (1)−(3) nonuniform. Such an approach was implemented, for example, in [1, 2], where a particle method for computing the transport equation was combined with a finite volume scheme for the shallow water equations. Other methods are also available. For example, a well-developed approach is based on finite-difference TVD schemes [3−6]. Additionally, pollutant transport in shallow water can be simulated using kinetic algorithms [7, 8], Godunov's schemes [9], finite-volume type methods [10], Lax−Friedrichs schemes combined with a central difference approximation for the transport equation [11], and others.

In this paper, for the simulation of passive scalar transport in shallow water, we propose a new uniform algorithm based on joint solution of the fluid dynamics equations and the transport equation. The system under consideration is solved as a whole by applying the quasi-gasdynamic approach [12−14].

An algorithm for constructing a regularized transport equation is described in Section 2. Specific tests for validating the numerical algorithm are presented in Sections 3 and 4. In the case of one-dimensional flows, these are pollutant transport by flow over a nonflat bottom [1], the classical Riemann problem [1, 4, 8], and the Riemann rarefaction problem [8]. In the last case, the exact solution for the transport equation is a stationary steplike concentration distribution, which is difficult to reproduce in numerical computations. An additional difficulty is that the formation of a dry-bed zone in the central part of the computational domain has to be described in this problem.

Two-dimensional tests are considered in Sections 4 and 5. They include examples given in [2], namely, the break of a symmetric dam on a flat bottom, which is also addressed in [4], and dam break on a nonflat bottom with a source. More specifically, the system of transport equations in shallow water with a source term is solved in Section 5. Problems with a source term are important, since they are used to simulate, for example, tanker accidents in a coastal zone and the spread of pollutant along the shore and in adjacent areas.

The problem of reproducing the dynamics of currents in Lake Vallunden, Spitsbergen, is addressed in Section 6. We present simulation results explaining experimental data obtained in the course of lake studies by researchers from the Shirshov Institute of Oceanology of the Russian Academy of Sciences [15, 16].

It should be noted that the difficulties associated with solving the passive scalar transport equation within the framework of fluid dynamics equations are manifested in both the shallow water model and the case of viscous incompressible fluids. A possible way out as applied to the SW equations is demonstrated in this paper. To conclude, we describe a method for regularizing the passive scalar transport equation for viscous incompressible fluid equations.

2. CONSTRUCTION OF A SYSTEM OF SMOOTHED EQUATIONS

We consider the system of regularized shallow water equations (referred to hereinafter as RSWE) described in [17]:

$$\frac{\partial h}{\partial t} + \text{div } \mathbf{j_m} = 0, \tag{5}$$

$$\frac{\partial (h\mathbf{u})}{\partial t} + \text{div} (\mathbf{j}_m \otimes \mathbf{u}) + \nabla \frac{gh^2}{2} = h^* (\mathbf{f} - g\nabla b) + \text{div } \Pi, \tag{6}$$

$$h^* = h - \tau \text{div} (h\mathbf{u}), \tag{7}$$

$$\mathbf{j}_m = h (\mathbf{u} - \mathbf{w}), \tag{8}$$

$$\mathbf{w} = \frac{\tau}{h} [\text{div} (h\mathbf{u} \otimes \mathbf{u}) + gh\nabla (b + h) - h\mathbf{f}], \tag{9}$$

$$\Pi = \Pi_{NS} + \tau \mathbf{u} \otimes [h(\mathbf{u} \cdot \nabla)\mathbf{u} + gh\nabla (b + h) - h\mathbf{f}] + \tau I [gh \text{ div} (h\mathbf{u})], \tag{10}$$

where $\tau > 0$ is a regularization parameter having the dimension of time; Π_{NS} is the Navier−Stokes viscous stress tensor, which, in some problems, if necessary, can be treated as an additional regularizer and can be included or dropped (see, e.g., [17, 18]); and μ is the kinematic viscosity of the fluid, which is treated as artificial and is computed in terms of the parameter τ:

$$\Pi_{NS} = \mu \frac{h}{2} [(\nabla \otimes \mathbf{u}) + (\nabla \otimes \mathbf{u})^T], \quad \mu = \tau gh. \tag{11}$$

System (5)−(10) is supplemented with a regularized transport equation. For this purpose, we write Eq. (3) in integral form, integrate it, and average over the time interval from t to $t + \Delta t$ to obtain

$$\frac{\widehat{C}\widehat{h} - Ch}{\Delta t} + \frac{1}{\Delta t} \int\limits_{t}^{t+\Delta t} \text{div} (\mathbf{u}Ch) dt' = \frac{1}{\Delta t} \int\limits_{t}^{t+\Delta t} \text{div} (Dh\nabla C) dt',$$

where $\widehat{C}$ and $\widehat{h}$ are taken at the time $t + \Delta t$. Applying the mean value theorem yields

$$\frac{\widehat{C}\widehat{h} - Ch}{\Delta t} + \text{div}(\mathbf{u}^* C^* h^*) = \text{div}(Dh^*\nabla C^*). \tag{12}$$

The quantities $h^*(\mathbf{x},t) = h(\mathbf{x},t^*)$, $\mathbf{u}^*(\mathbf{x},t) = \mathbf{u}(\mathbf{x},t^*)$, and $C^*(\mathbf{x},t) = C(\mathbf{x},t^*)$ are determined at an intermediate time level: $t < t^* < \Delta t$. Their values over a short time interval Δt are assumed to vary little, and, assuming that the corresponding derivatives exist and are sufficiently smooth, these variations can be estimated by the first term of the series expansion with respect to time.

A regularizer is constructed as follows. The above quantities at the time level t^* are represented by the first-order series terms in time, where $\tau \sim \Delta t$:

$$\mathbf{u}^* = \mathbf{u} + \tau \frac{\partial \mathbf{u}}{\partial t}, \quad h^* = h + \tau \frac{\partial h}{\partial t}, \quad C^* = C + \tau \frac{\partial C}{\partial t}.$$

Next, by analogy with the construction of QGD equations, the time derivatives are expressed using the original system of equations. Consider $\frac{\partial C}{\partial t}$ in Eq. (3). Expanding the time derivative yields

$$h\frac{\partial C}{\partial t} + C\frac{\partial h}{\partial t} = -\text{div} (\mathbf{u}hC) + \text{div} (Dh\nabla C) = -C\text{div} (\mathbf{u}h) - (\mathbf{u}h \cdot \nabla C) + \text{div} (Dh\nabla C),$$

where, after substituting $\frac{\partial h}{\partial t}$ from (1), we obtain

$$\frac{\partial C}{\partial t} = -(\mathbf{u} \cdot \nabla C) + \frac{1}{h}\operatorname{div}(Dh\nabla C),$$

whence

$$C^* = C - \tau(\mathbf{u} \cdot \nabla C) + O(\tau^2),$$

where the term with τD is negligibly small as compared with $O(\tau)$.

It follows from (5) that

$$h^*\mathbf{u}^* = h(\mathbf{u} - \mathbf{w}) + O(\tau^2).$$

Then, returning to Eq. (12), omitting terms of order $O(\tau^2)$, and replacing the difference time derivative by its differential counterpart, we finally obtain the regularized transport equation

$$\frac{\partial Ch}{\partial t} + \operatorname{div}(\mathbf{j}_m C) = \operatorname{div}(Dh\nabla C + \tau \mathbf{u}h(\mathbf{u} \cdot \nabla C)). \tag{13}$$

Smoothed over time, Eq. (4) becomes

$$\frac{\partial C}{\partial t} + \operatorname{div}\left(C\left[\mathbf{u} - \mathbf{w} + \tau\frac{\mathbf{u}}{h}(\mathbf{u} \cdot \nabla h)\right]\right) = \operatorname{div}(D\nabla C + \tau\mathbf{u}(\mathbf{u} \cdot \nabla C)).$$

In the subsequent computations, as was indicated above, Eq. (13) is used as a smoothed transport equation.

An algorithm based on only regularized hydrodynamic equations without using the regularized transport equation turns out to be poorly stable. Its comparison with the version proposed above can be found in [19].

3. NUMERICAL SIMULATION OF ONE-DIMENSIONAL FLOWS

In the case of plane one-dimensional flows without external forces, the RSWE system, together with the transport equation, has the form

$$\frac{\partial h}{\partial t} + \frac{\partial j_m}{\partial x} = 0, \tag{14}$$

$$\frac{\partial hu}{\partial t} + \frac{\partial j_m u}{\partial x} + \frac{\partial}{\partial x}\left(\frac{gh^2}{2}\right) + gh\frac{\partial b}{\partial x} = \frac{\partial \Pi}{\partial x}, \tag{15}$$

$$\frac{\partial Ch}{\partial t} + \frac{\partial}{\partial x}(j_m C) = \frac{\partial}{\partial x}\left(h(D + \tau u^2)\frac{\partial C}{\partial x}\right), \tag{16}$$

where

$$j_m = h(u - w), \tag{17}$$

$$w = \frac{\tau}{h}\left[\frac{\partial(hu^2)}{\partial x} + gh\frac{\partial}{\partial x}(h + b)\right], \tag{18}$$

$$\Pi = \tau hu\left[u\frac{\partial u}{\partial x} + g\frac{\partial}{\partial x}(h + b)\right] + \tau gh\frac{\partial(hu)}{\partial x}. \tag{19}$$

In this section, we do not use additional viscosity (11), i.e., $\mu = 0$.

The regularized SW equations (14)−(19) are solved numerically by applying methods similar to those developed for quasi-gasdynamic equations [17]. Namely, we use a time-explicit difference scheme with all spatial derivatives approximated by central differences. The superscript k indicates that the considered quantity is taken at the kth time step. For notational simplicity, it is omitted from the right-hand side of the equations, where the values of all quantities are taken at the current time step, i.e., $u_{i+1/2} = u_{i+1/2}^k$. The values of the sought variables $h(x,t)$, $u(x,t)$, and $C(x,t)$ are specified at spatial grid points i. The values of

variables at half-integer grid points $i + 1/2$ are determined as the arithmetic mean of their values at neighboring points:

$$b_{i+1/2} = \frac{b_i + b_{i+1}}{2}, \quad \tau_{i+1/2} = \frac{\tau_i + \tau_{i+1}}{2},$$

$$h_{i+1/2} = \frac{h_i + h_{i+1}}{2}, \quad u_{i+1/2} = \frac{u_i + u_{i+1}}{2}, \quad C_{i+1/2} = \frac{C_i + C_{i+1}}{2}; \qquad (20)$$

$$w_{i+1/2} = \frac{\tau_{i+1/2}}{h_{i+1/2}}\left(\frac{h_{i+1}u_{i+1}^2 - h_i u_i^2}{\Delta x} + gh_{i+1/2}\frac{h_{i+1} + b_{i+1} - h_i - b_i}{\Delta x}\right);$$

$$\Pi_{i+1/2} = \tau_{i+1/2}u_{i+1/2}h_{i+1/2}\left(u_{i+1/2}\frac{u_{i+1} - u_i}{\Delta x} + g\frac{h_{i+1} + b_{i+1} - h_i - b_i}{\Delta x}\right) + \tau_{i+1/2}gh_{i+1/2}\frac{h_{i+1}u_{i+1} - h_i u_i}{\Delta x}; \qquad (21)$$

$$j_{m,i+1/2} = h_{i+1/2}\left(u_{i+1/2} - w_{i+1/2}\right); \qquad (22)$$

$$\frac{h_i^{k+1} - h_i^k}{\Delta t} + \frac{j_{m,i+1/2} - j_{m,i-1/2}}{\Delta x} = 0; \qquad (23)$$

$$\frac{h_i^{k+1}u_i^{k+1} - h_i^k u_i^k}{\Delta t} + \frac{u_{i+1/2}j_{m,i+1/2} - u_{i-1/2}j_{m,i-1/2}}{\Delta x} + \frac{g}{2}\frac{h_{i+1/2}^2 - h_{i-1/2}^2}{\Delta x} = -gh_i^*\frac{b_{i+1/2} - b_{i-1/2}}{\Delta x} + \frac{\Pi_{i+1/2} - \Pi_{i-1/2}}{\Delta x}; \qquad (24)$$

$$\frac{C_i^{k+1}h_i^{k+1} - C_i^k h_i^k}{\Delta t} + \frac{j_{m,i+1/2}C_{i+1/2} - j_{m,i-1/2}C_{i-1/2}}{\Delta x}$$
$$= \frac{1}{\Delta x}\left(h_{i+1/2}\frac{C_{i+1} - C_i}{\Delta x}(D + \tau_{i+1/2}u_{i+1/2}^2) - h_{i-1/2}\frac{C_i - C_{i-1}}{\Delta x}(D + \tau_{i-1/2}u_{i-1/2}^2)\right). \qquad (25)$$

Here,

$$h_i^* = h_i - \tau_i\frac{h_{i+1/2}u_{i+1/2} - h_{i-1/2}u_{i-1/2}}{\Delta x}. \qquad (26)$$

The stability of the numerical algorithm is ensured by terms with a regularization coefficient τ, which is defined as

$$\tau = \alpha\frac{l}{c}; \qquad (27)$$

here, l is the characteristic length of a spatial cell, which is used in the numerical algorithm, for example, in the form $l = \sqrt{s}$, where s is the area of a cell; $c = \sqrt{gh}$ is the propagation velocity of long waves; and α is a numerical coefficient specified depending on the required accuracy and stability of the computations. As a rule, $0 < \alpha < 1$, and, as a baseline value, we can choose $\alpha = 0.5$. In the one-dimensional computations, the characteristic length is set equal to the mesh spatial step $l = \Delta x$.

The stability condition has the form the Courant−Friedrichs−Lewy condition, where the time step is given by the formula

$$\Delta t = \beta\left(\frac{\Delta x}{c}\right)_{min}, \quad 0 < \beta < 1. \qquad (28)$$

In all tests considered below, the Courant number β is specified as $\beta = 0.1$ (unless otherwise stated). In all test problems, we use $D = 0$ and, additionally, flow drift conditions for the height, velocity, and concentration are set on the left and right boundaries (unless otherwise stated):

$$\frac{\partial h}{\partial x} = 0, \quad \frac{\partial u}{\partial x} = 0, \quad \frac{\partial C}{\partial x} = 0.$$

Below, we consider examples of test problems solved numerically by applying the difference algorithm described above. Uniform spatial grids were used in all computations. Since only model problems were considered, all quantities were dimensionless. Additional results for one-dimensional flows can be found in [19].
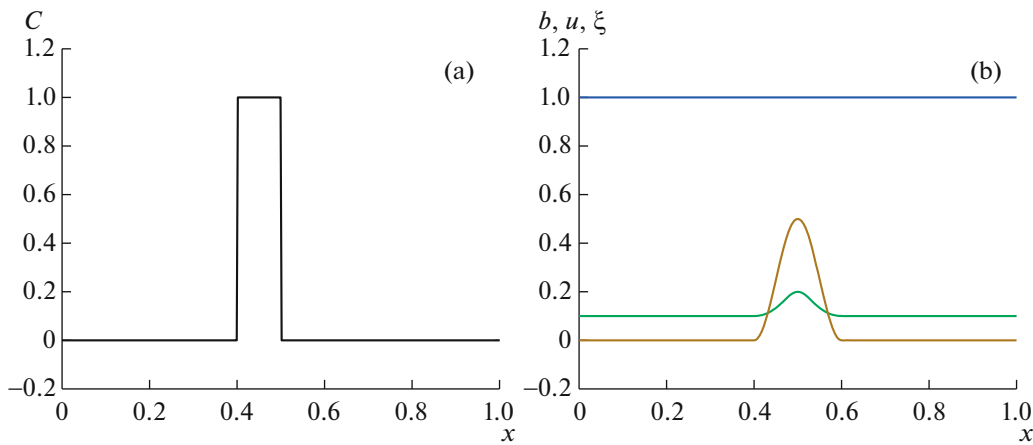
Fig. 2. Initial conditions: (a) concentration distribution and (b) distributions of the free surface elevation, velocity, and bottom topography.
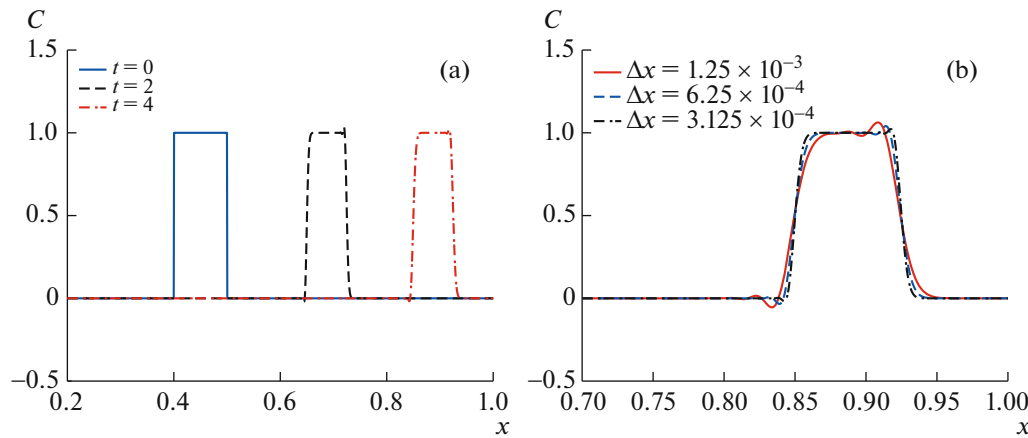

Fig. 3. Concentration distribution, $\alpha = 0.5$, $\beta = 0.1$ (a) at various times, $\Delta x = 3.125 \times 10^{-4}$ and (b) for various values of Δx, $t = 4$.

3.1. Pollutant Advection over a Nonflat Bottom

The example is taken from [1]. The initial conditions are shown in Fig. 2; the computational domain is $x \in [0,1]$. Initially, the free surface elevation is $\xi(x,0) \equiv 1$. The initial discharge is $Q(x,0) = h(x,0)u(x,0) = 0.1$, and $g = 1$. The initial pollutant distribution is specified as $C(x,0) = 1$ on the interval $[0.4, 0.5]$ and $C(x,0) = 0$ in the rest of the domain. The bottom elevation function is defined as

$$b(x) = \begin{cases} 0.25(\cos(10\pi(x - 0.5)) + 1), & 0.4 \leq x \leq 0.6, \\ 0, & x \notin [0.4, 0.6]. \end{cases}$$

It is easy to see that the regularizing additions involved in Eq. (16) are nonzero only in domains with non-zero gradients of velocity and pollutant concentration. It was noted that, if the numerical solution initially exhibits oscillations due to the inaccurately specified initial conditions for concentration, then, in solution domains with a constant concentration or velocity, these oscillations do not flatten out with time and are transported by the flow without change. Accordingly, for the correct simulation of the problem, the initial perturbation has to be specified accurately. For this purpose, the initial perturbation is smoothed over the grid, namely, the initial concentration values at the discontinuity boundary are specified at three points: the left (C_l) and right (C_r) boundaries of the discontinuity and a point between them as the half-sum of the boundary values: $\dfrac{C_l + C_r}{2} = 0.5$.
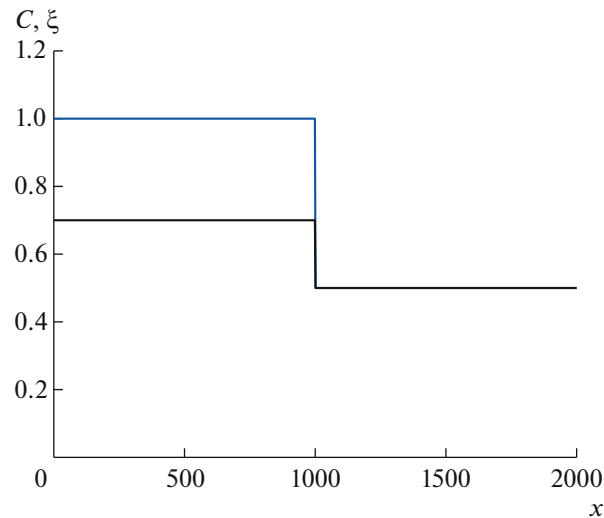
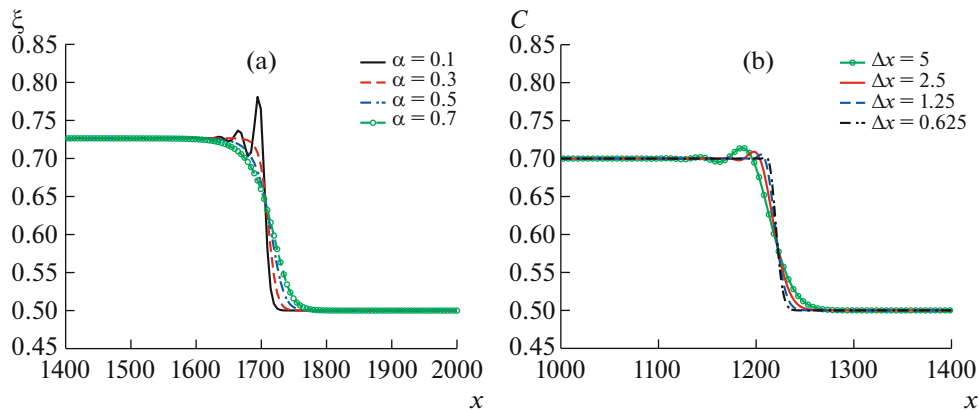**Fig. 4.** Initial distributions of the concentration and free surface elevation.

Fig. 5. Distributions at $t = 240$, $\beta = 0.1$: (a) free surface elevation for various α and $\Delta x = 5$; (b) concentration for refined meshes and $\alpha = 0.3$.

According to [1], the model solution of this problem is the initial perturbation of the pollutant concentration displacing to the right with time with the preservation of its height $C = 1$.

Figure 3a shows the results obtained for $\Delta x = 3.125 \times 10^{-4}$ and $\alpha = 0.5$ at $t = 0$, 2, and 4.

In [1] a finite volume (FV) method was compared with a finite-volume-particle (FVP) method (finite volume scheme combined with a particle method), where the number of pollutant particles was equal to 20. Both methods were computed using a central scheme with upwind differences on a grid with $\Delta x = 0.005$. A comparison with the RSWE results shows that they agree with the results produced by the FV and FVP models in [1].

Figure 3b displays the results for $\alpha = 0.5$, $\beta = 0.1$, and various Δx. It can be seen that the solution converges under mesh refinement.

3.2. Dam Break on a Flat Bottom

Consider the classical Riemann problem on a flat bottom; its formulation is taken from [8]. In this problem, the pollutant concentration and the fluid level have a discontinuity at the point of dam break (see Fig. 4); the computational domain is $x \in [0, 2000]$. The initial values are specified as $(h, u, C) = (1.0, 0, 0.7)$, $x \in [0, 1000]$; $(h, u, C) = (0.5, 0, 0.5)$, $x \in [1000, 2000]$. As in the previous case, the
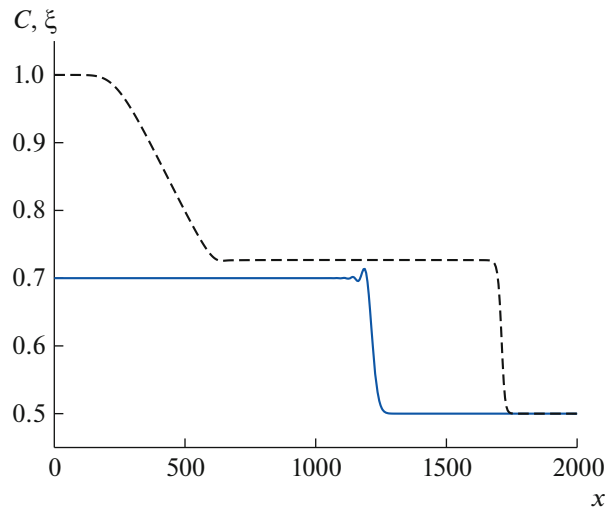
Fig. 6. Distributions of the concentration and free surface elevation at $t = 240$ for $\Delta x = 5$, $\alpha = 0.3$, and $\beta = 0.1$.
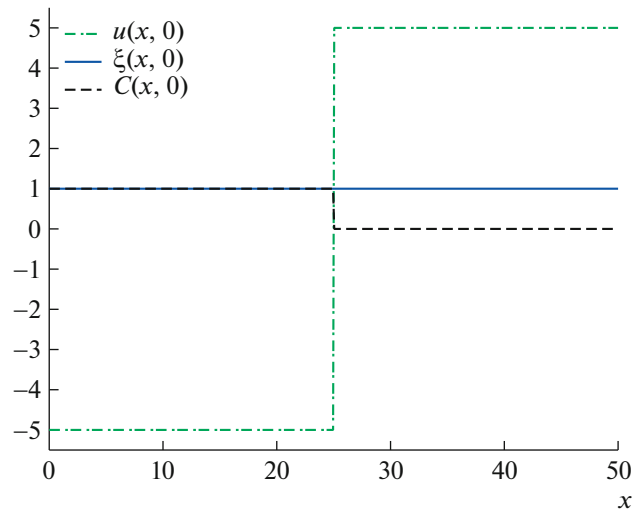

Fig. 7. Initial distributions of velocity, concentration, and free surface elevation.

concentration and the height at the discontinuity boundary are specified at three points: the left and right boundaries of the discontinuity and a point between them as the half-sum of the boundary values.

The numerical solution of the problem for ξ consists of three plane zones, namely, two original inactive zones at the edges and an intermediate zone, which are separated by two simple waves: a rarefaction wave propagating to the left and a shock wave propagating to the right, while the concentration jump is transported at the velocity of the intermediate plane zone.

Figure 5a presents the numerical solution for the water level as a function of the regularization coefficient α for $\Delta x = 5$. As $\alpha = 0.1$ is approached, oscillations arise and the stability of the numerical solution is violated. In what follows, $\alpha = 0.3$.

Figure 5b demonstrates the convergence of the solution for pollutant concentration under mesh refinement.

In [8] the results were obtained by applying a second-order accurate kinetic scheme with two stages in time and $\Delta x = 20$. Figure 6 shows that they nearly coincide with the results obtained using the regularized equations with a first-order accurate scheme.
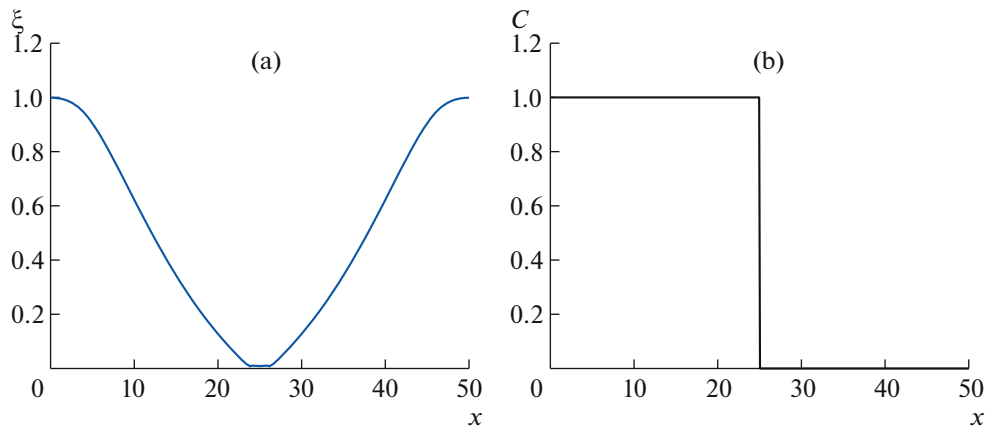
Fig. 8. Numerical results for $t = 2.5$, $\Delta x = 0.1$, and $\alpha = 0.3$: distributions of (a) free surface elevation and (b) concentration.

3.3. Riemann Rarefaction Problem

According to the formulation in [4], we considered the domain $x \in [0, 50]$. The initial conditions were specified so as to produce two rarefaction waves propagating in opposite directions from the discontinuity center located at $x_0 = 25$ (see Fig. 7). The values to the left of the discontinuity were specified as $(h, u, C) = (1, -5, 1)$, $x \in [0, 25]$. The values to the right were $(h, u, C) = (1, 5, 0)$, $x \in [25, 50]$. The computation time was $t = 2.5$. The velocity and concentration at the discontinuity boundary were specified at two points, i.e., without intermediate smoothing.

At the time $t = 2.5$, a dry-bed zone was formed in the center of the domain. Dry-bed areas were treated using a widespread approach, which is described in detail, for example, in [20]. This approach involves a cutoff parameter ε specifying the minimum water layer thickness h, which was computed using the finite-difference algorithm.

In this problem, the bottom is flat and the cutoff parameter is specified as the constant $\varepsilon = 0.001$.

In the dry-bed zones, the fluid is at rest, so, for small h, the following constraints are imposed on τ and u:

$$\tau = \begin{cases} \alpha \Delta x / \sqrt{gh}, & h > \varepsilon, \\ 0, & h \leq \varepsilon, \end{cases} \tag{29}$$

$$\text{if } h < \varepsilon, \quad h = \varepsilon \text{ and } u = 0. \tag{30}$$

A similar problem without allowance for pollutant transport was considered within the framework of the RSWE; its solution and the method for calculating wet/dry zones can be found in [20].

In [4] it was indicated that the exact solution for the pollutant concentration C in this problem is a stationary discontinuity, which is difficult to reproduce by most numerical schemes.

The resulting distributions of ξ and C at the time $t = 2.5$ for $\Delta x = 0.1$ and $\alpha = 0.3$ are presented in Fig. 8. It should be emphasized that the algorithm we used reproduces the exact solution for the concentration distribution in the case of any mesh over the entire computation time.

4. DIFFERENCE ALGORITHM FOR SIMULATION OF TWO-DIMENSIONAL FLOWS AND AN EXAMPLE OF DAM BREAK COMPUTATION

A finite-difference algorithm for simulating two-dimensional flows is constructed similar to the one-dimensional case. System (5)–(13) is approximated using the finite volume method with all spatial derivatives approximated by central differences up to second-order accuracy. Finite-difference schemes for RSWE were repeatedly published; they can be found, for example, in [17–20]. Below, we describe only the approximation of the transport equation. Note that, for the computation of two-dimensional flows, the Navier–Stokes regularizer (11) was not dropped.
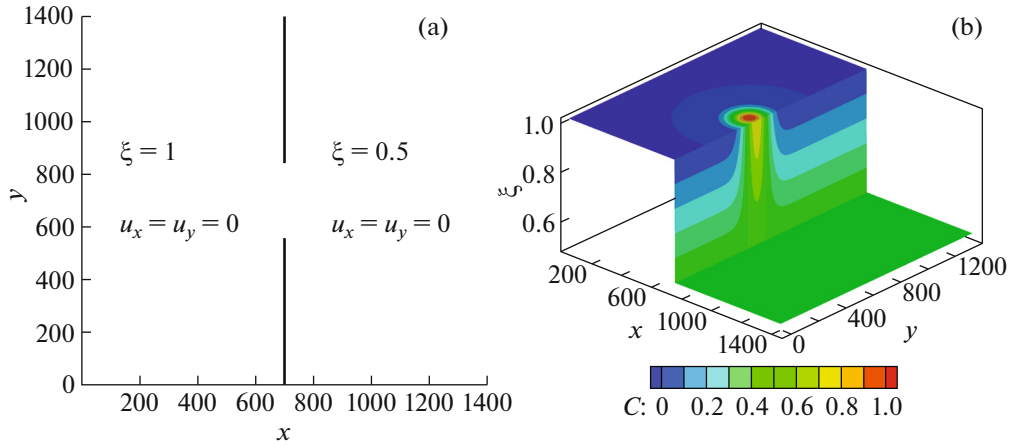
Fig. 9. Initial distributions of (a) free surface elevation and velocity and (b) free surface elevation with imposed concentration distribution.

In plane geometry, the concentration equation in the RSWE system is written as

$$\frac{\partial Ch}{\partial t} + \frac{\partial j_{mx}C}{\partial x} + \frac{\partial j_{my}C}{\partial y} = \frac{\partial}{\partial x}\left(h(D + \tau u_x^2)\frac{\partial C}{\partial x} + \tau u_x u_y h \frac{\partial C}{\partial y}\right) + \frac{\partial}{\partial y}\left(h(D + \tau u_y^2)\frac{\partial C}{\partial y} + \tau u_x u_y h \frac{\partial C}{\partial x}\right). \quad (31)$$

The corresponding difference implementation has the form

$$\hat{C}\hat{h} = Ch - \frac{\Delta t}{\Delta x}(j_{i+1/2,j}^x C_{i+1/2,j} - j_{i-1/2,j}^x C_{i-1/2,j}) - \frac{\Delta t}{\Delta y}(j_{i,j+1/2}^y C_{i,j+1/2} - j_{i,j-1/2}^y C_{i,j-1/2})$$

$$+ \frac{\Delta t}{\Delta x}\left(h_{i+1/2,j}\frac{C_{i+1,j} - C_{i,j}}{\Delta x}(D + \tau_{i+1/2,j}(u_{i+1/2,j}^x)^2) + \tau_{i+1/2,j}u_{i+1/2,j}^x u_{i+1/2,j}^y h_{i+1/2,j}\frac{C_{i+1/2,j+1/2} - C_{i+1/2,j-1/2}}{\Delta y}\right.$$

$$\left. - h_{i-1/2,j}\frac{C_{i,j} - C_{i-1,j}}{\Delta x}(D + \tau_{i-1/2,j}(u_{i-1/2,j}^x)^2) - \tau_{i-1/2,j}u_{i-1/2,j}^x u_{i-1/2,j}^y h_{i-1/2,j}\frac{C_{i-1/2,j+1/2} - C_{i-1/2,j-1/2}}{\Delta y}\right)$$

$$+ \frac{\Delta t}{\Delta y}\left(h_{i,j+1/2}\frac{C_{i,j+1} - C_{i,j}}{\Delta y}(D + \tau_{i,j+1/2}(u_{i,j+1/2}^y)^2) + \tau_{i,j+1/2}u_{i,j+1/2}^x u_{i,j+1/2}^y h_{i,j+1/2}\frac{C_{i+1/2,j+1/2} - C_{i-1/2,j+1/2}}{\Delta x}\right.$$

$$\left. - h_{i,j-1/2}\frac{C_{i,j} - C_{i,j-1}}{\Delta y}(D + \tau_{i,j-1/2}(u_{i,j-1/2}^y)^2) - \tau_{i,j-1/2}u_{i,j-1/2}^x u_{i,j-1/2}^y h_{i,j-1/2}\frac{C_{i+1/2,j-1/2} - C_{i-1/2,j-1/2}}{\Delta x}\right).$$

To demonstrate the efficiency of the two-dimensional algorithm, we used two benchmark tests, whose numerical results are described below. Since the problems are model ones, all quantities are dimensionless. Some preliminary results in these cases are given in [19].

4.1. Break of a Symmetric Dam on a Flat Bottom

The formulation and numerical simulation of this problem are described in [2, 4].

The computational domain is the square $[0,1400] \times [0,1400]$ separated by a wall in the middle. At the initial time, a central section of the wall collapses and a flow develops due to the difference in the water levels. Figure 9 shows the initial data for the free surface elevation, velocity, and concentration. The water follows through a hole located between the coordinates $y = 560$ and $y = 840$; the coordinate of the wall is $x = 700$.

The initial conditions for the pollutant concentration are specified by the function

$$C(x, y, t = 0) = \begin{cases} e^{-0.0001[(x-650)^2 + (y-600)^2]}, & 0 \leq x \leq 700, \quad 0 \leq y \leq 1400, \\ 0.5, & 700 \leq x \leq 1400, \quad 0 \leq y \leq 1400. \end{cases}$$

Note that the initial distribution of the pollutant concentration is asymmetrical about the wall.
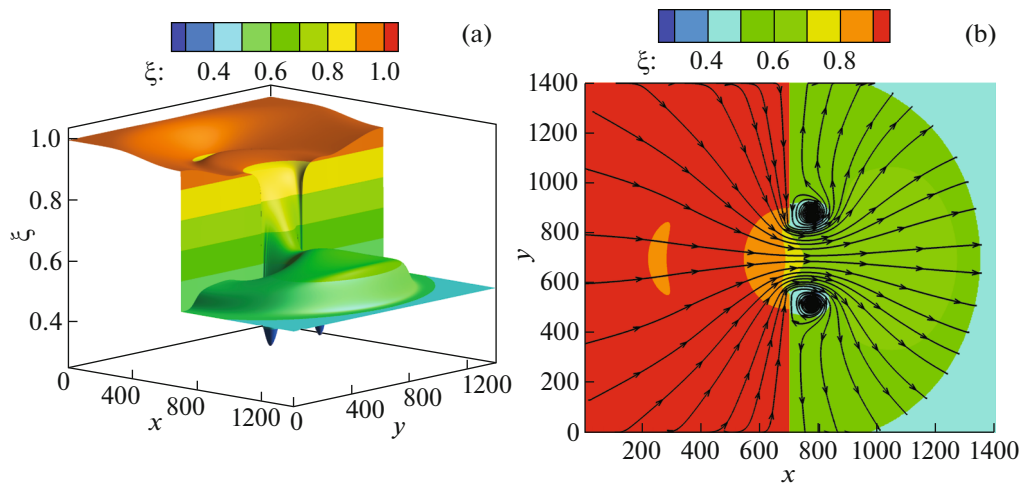
Fig. 10. Numerical results for the free surface elevation distribution: (a) schematic three-dimensional view and (b) contour lines of free surface elevation and streamlines.
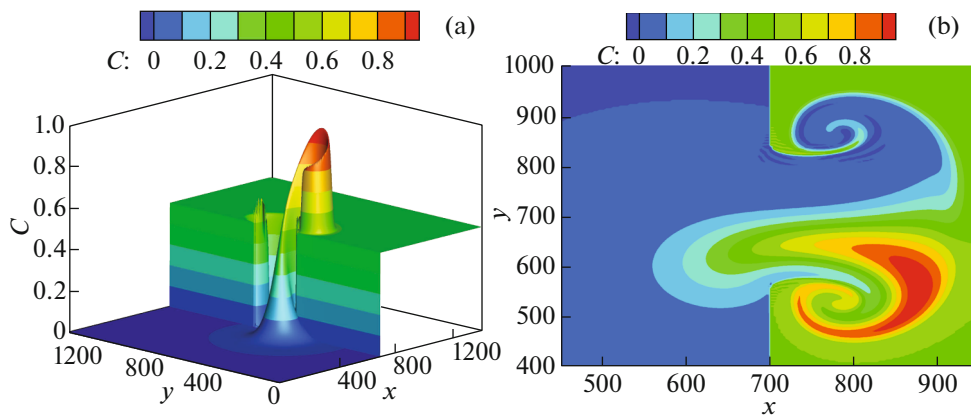

Fig. 11. Numerical results for the pollutant concentration: (a) schematic three-dimensional view and (b) projection onto the Oxy plane.

At the boundaries corresponding to $x = 0$ and $x = 1400$, we set the flow drift conditions

$$\frac{\partial h}{\partial x} = 0, \quad \frac{\partial C}{\partial x} = 0, \quad \frac{\partial u_x}{\partial x} = 0, \quad \frac{\partial u_y}{\partial x} = 0.$$

Reflection conditions are specified on the walls at $y = 0$ and $y = 1400$:

$$\frac{\partial h}{\partial y} = 0, \quad \frac{\partial C}{\partial y} = 0, \quad \frac{\partial u_x}{\partial y} = 0, \quad u_y = 0,$$

and on the internal walls:

$$\frac{\partial h}{\partial x} = 0, \quad \frac{\partial C}{\partial x} = 0, \quad u_x = 0, \quad \frac{\partial u_y}{\partial x} = 0.$$

Figures 10 and 11 present the results obtained at $t = 200$ for the coefficients $\alpha = 0.5$ and $\beta = 0.2$. The grid sizes are $N_x = N_y = 500$, which corresponds to $\Delta x = \Delta y = 2.8$. The same meshes were used in [2, 4].

In [2] a finite volume (FV) method was compared with a finite-volume-particle (FVP) method (finite volume scheme combined with a particle method). Accordingly, in what follows, the RSWE results are compared with those based on these two models.

The numerical results agree well with [2, 4]. As α is reduced to 0.2, the vortex amplitude increases, which agrees with the flow pattern presented in [2, 4]. The solution for the free surface elevation in Fig. 10 clearly exhibits a circular hydraulic jump and vortices on both sides of the discontinuity. Similarly, for the concentration in Fig. 11, the front positions and the structures inside the vortices agree with [2].

There are insignificant oscillations of the pollutant concentration in a small vortex, which are also observed in [2] for the FV method. In the case of FVP, the vortex is unnaturally smoothed, which raises doubts about the correctness of the solution obtained in [2].

5. DAM BREAK ON A NONFLAT BOTTOM WITH A SOURCE

In a similar manner, the RSWE system including pollutant transport was generalized to the case of a nonzero pollutant source by applying the quasi-gasdynamic approach. The SW equations with a pollutant source differ from the classical equations (1)−(4) by a mass source S on the right-hand side of Eq. (1) and by a pollutant source on the right-hand side of Eq. (3) or (4) (see, e.g., [4, 8]).

The RSWE system and the transport equation with a pollutant source, but without external forces have the form

$$\frac{\partial h}{\partial t} + \operatorname{div} \mathbf{j_m} = S, \tag{32}$$

$$\frac{\partial (h\mathbf{u})}{\partial t} + \operatorname{div}\left(\mathbf{j}_m \otimes \mathbf{u}\right) + \nabla \frac{gh^2}{2} = -gh^*\nabla b + \operatorname{div} \Pi, \tag{33}$$

$$\frac{\partial Ch}{\partial t} + \operatorname{div}\left(\mathbf{j}_m C\right) = \operatorname{div}\left(Dh\nabla C + \tau \mathbf{u}\left[(\mathbf{u}h \cdot \nabla C) + CS - T_s S\right]\right) + T_s S, \tag{34}$$

where

$$h^* = h - \tau\left(\operatorname{div}(h\mathbf{u}) - S\right), \tag{35}$$

$$\mathbf{j}_m = h\left(\mathbf{u} - \mathbf{w}\right), \tag{36}$$

$$\mathbf{w} = \frac{\tau}{h}\left[\operatorname{div}\left(h\mathbf{u} \otimes \mathbf{u}\right) + gh\nabla\left(b + h\right)\right], \tag{37}$$

$$\Pi = \Pi_{NS} + \tau \mathbf{u} \otimes \left[h\left(\mathbf{u} \cdot \nabla\right)\mathbf{u} + gh\nabla\left(b + h\right) + S\mathbf{u}\right] + \tau I\left[gh\left(\operatorname{div}\left(h\mathbf{u}\right) - S\right)\right]. \tag{38}$$

The notation is the same as in the RSWE. In addition, the equations involve the fluid source $S(\mathbf{x}, t)$ and the pollutant concentration T_s at the source S.

Regularizer (35)−(38) for system (32)−(34) was constructed taking into account the pollutant source in the system. The subsequent numerical experiments showed that the source term S involved in the formulas for additional dissipation does not influence the numerical solution of the problem considered below. Nevertheless, as was noted in [4, 8], the presence of a source term imposes nontrivial balance conditions and conservation laws, which fail to be satisfied in some schemes. To estimate the influence exerted by this factor on the solution of system (32)−(38), it is possible to generalize the energy estimate of the solution from [21].

The algorithm was tested using a benchmark problem given in [2].

In the square domain $[0, 1400] \times [0, 1400]$, there is a discontinuity of complex geometry, which starts to decay at $t = 0$. The initial distributions of depth and velocities are shown in Fig. 12. The boundary of two domains is described by the function

$$\Gamma(y) = \begin{cases} \min\left[500 + \dfrac{(y - 700)^2}{400}, 900\right], & 0 \le y \le 700, \\ 500, & 700 \le y \le 1400. \end{cases}$$

The bottom in this problem has the form of three elliptic Gaussians:

$$b(x, y) = 4.5\left[e^{-\kappa_1(x-800)^2 - \kappa_2(y-700)^2} + e^{-\kappa_2(x-600)^2 - \kappa_1(y-600)^2} + e^{-\kappa_2(x-1000)^2 - \kappa_1(y-700)^2}\right],$$
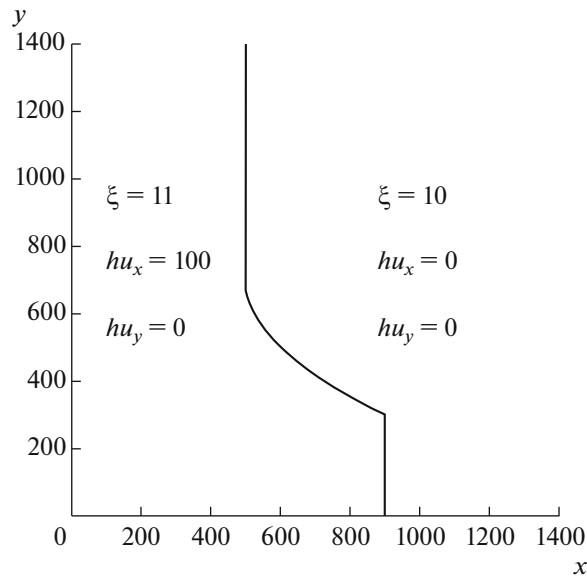
where $\kappa_1 = 10^{-4}$ and $\kappa_2 = 10^{-3}$.

Fig. 12. Initial distributions of the free surface elevation and discharges.
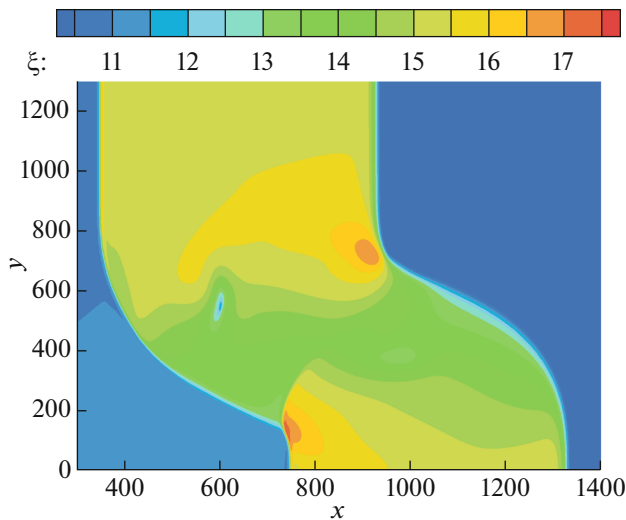

Fig. 13. Numerical results: contour lines of the free surface elevation.

Initially, the concentration is $C(x, y, t = 0) = 0$, but later, due to the presence of the source specified by the formula

$$S(x, y, t) = 0.5e^{-0.5(t-8)^2 - 0.00001(x+y-1300)^2 - 0.0005(x-y-100)^2}$$

with $T_s = 25$, the concentration C increases.

Flow drift conditions are set on the boundaries:

$$\frac{\partial h}{\partial \mathbf{n}} = 0, \quad \frac{\partial C}{\partial \mathbf{n}} = 0, \quad \frac{\partial u_n}{\partial \mathbf{n}} = 0, \quad \frac{\partial u_\tau}{\partial \mathbf{n}} = 0,$$

where the indices n and τ denote to the normal and tangential directions to the boundary of the domain, respectively.

Figures 13–15 present the simulation results at the time $t = 30$ for $\alpha = 0.5$, $\beta = 0.2$, and $N_x = N_y = 500$, which correspond to $\Delta x = \Delta y = 2.8$.
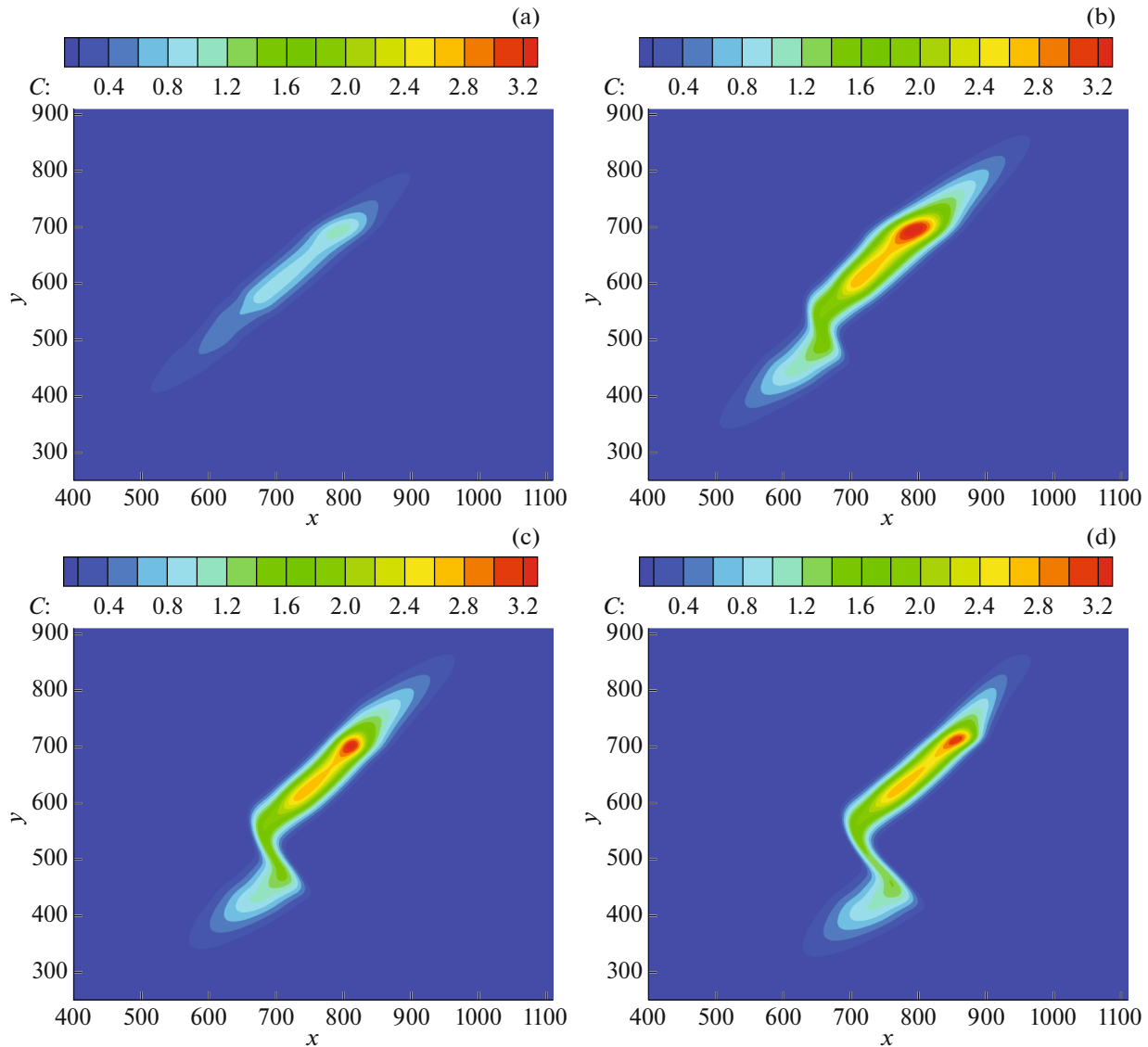
Fig. 14. RSWE: Contour lines of the pollutant concentration distribution at various times: (a) $t = 7.5$, (b) $t = 15$, (c) $t = 22.5$, and (d) $t = 30$.

The FV and FVP methods with the same grid size $N_x = N_y = 500$ were compared in [2]. Accordingly, the RSWE numerical results are compared with these two models.

Figure 13 shows the computed free surface elevation. It can be seen that the collision of the curved shock wave in the initial distribution with the rough bottom leads to rather complex wave structures. The resulting distribution agrees with the one presented in [2].

Figure 14 displays the pollutant concentration based on RSWE at the same times as in [2]. It should be emphasized that both results were obtained on identical spatial grids, but the RSWE method is first-order accurate in space, while the method of [2] is at least second-order accurate. A visual comparison of the results of RSWE and [2] shows that they are in close agreement.

In Fig. 15, the numerical results for the concentration presented as the two-dimensional projection onto the (C, y) axes are compared by imposing the plots. It can be seen that the RSWE result (obtained with $\beta = 0.2$, $\alpha = 0.5$, $N_x = N_y = 500$) lies between the FV and FVP plots from [2]. As in the dam break problem presented above, the FVP method of [2] yields too smoothed results.
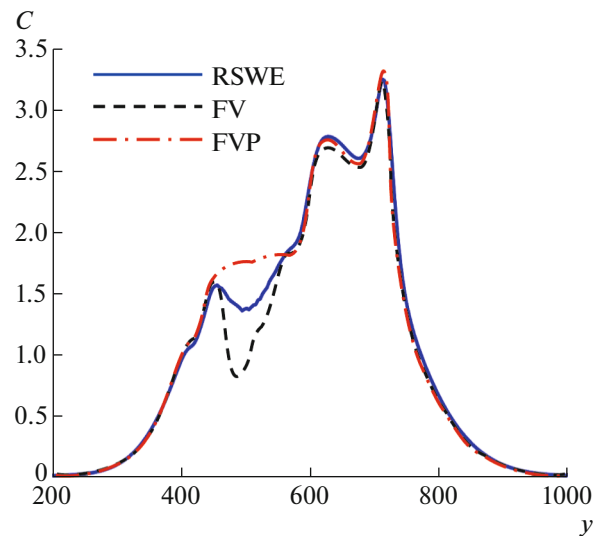
Fig. 15. Comparison of the 2D projections of the pollutant concentration ($C(y)$) at the time $t = 30$ produced by RSWE ($\beta = 0.2$, $\alpha = 0.5$, $N_x = N_y = 500$) and FV and FVP from [2].
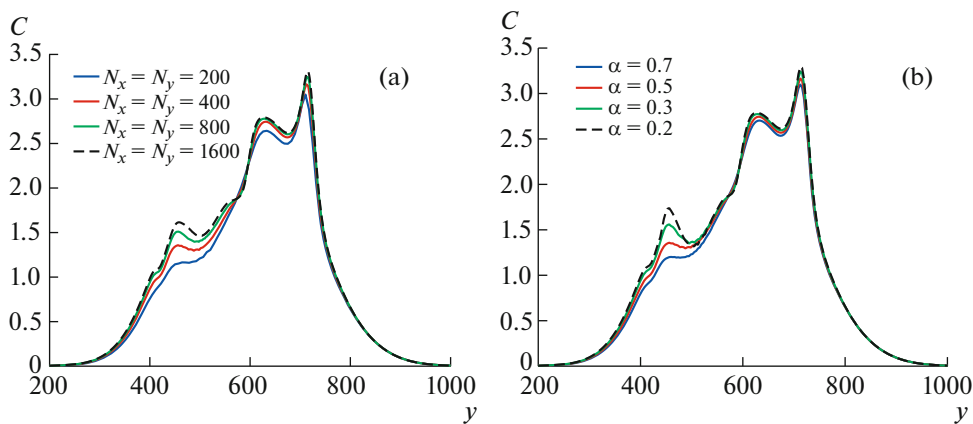

Fig. 16. RSWE: 2D projection of the pollutant concentration $C(y)$, $\beta = 0.2$, for (a) various meshes and $\alpha = 0.5$ and for (b) various values of α and $N_x = N_y = 400$.

Figure 16 shows the numerical solution as a function of the mesh size (for $\beta = 0.2$, $\alpha = 0.5$) and of the parameter α (for $N_x = N_y = 400$, $\beta = 0.2$). Clearly, the numerical solution converges under the spatial mesh refinement and the features of the concentration distribution are better resolved as the regularization parameter α is reduced.

6. COMPUTATION OF THE CIRCULATION IN LAKE VALLUNDEN

Consider Lake Vallunden, Spitsbergen, 77°53′ N, 16°46′ E [15, 16] (see Fig. 17). The size of the lake is about 1300 by 700 m. The bottom is rather smooth with a quickly increasing depth. In the center of the lake, the depth is about 10−12 m. The lake is connected to a coastal inlet—a fjord—through a narrow channel about 1 m deep. The strong tidal currents with water level oscillations in the fjord reaching 2 m give rise to an unsteady current in the channel with velocities of up to 1 m/s. It is well known that the current flowing into the lake is cooler than the lake water. This is a real-world problem, so all quantities are given in SI units, except for the pollutant concentration (see the explanation below).

The goal was to compute the currents in the lake arising during flood/ebb currents from the fjord. Additionally, we determined how the inflow affects the ice formation in cold time. A simplified model of
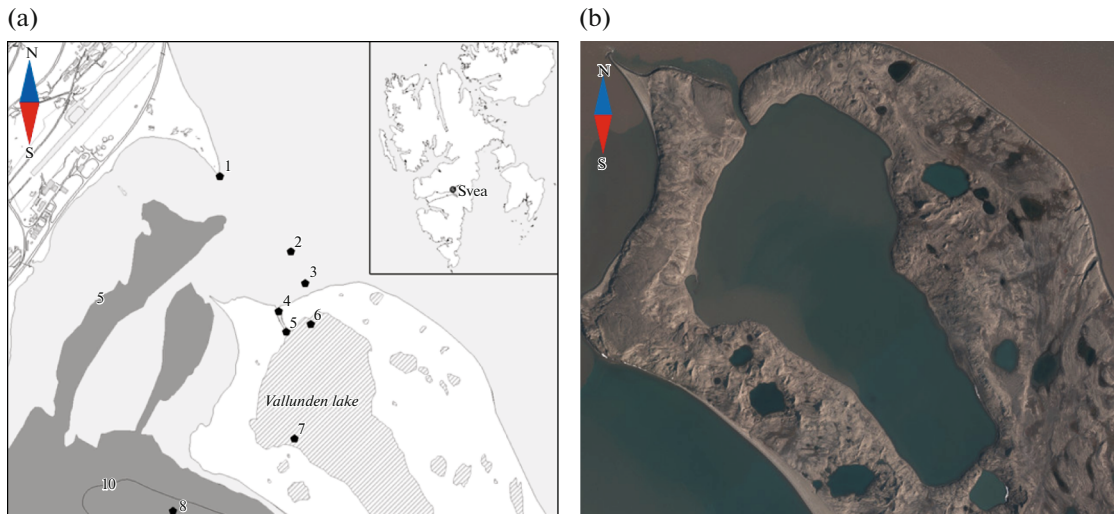
Fig. 17. Lake Vallunden: (a) schematic map of the lake from [15] and (b) satellite image taken from the Internet.
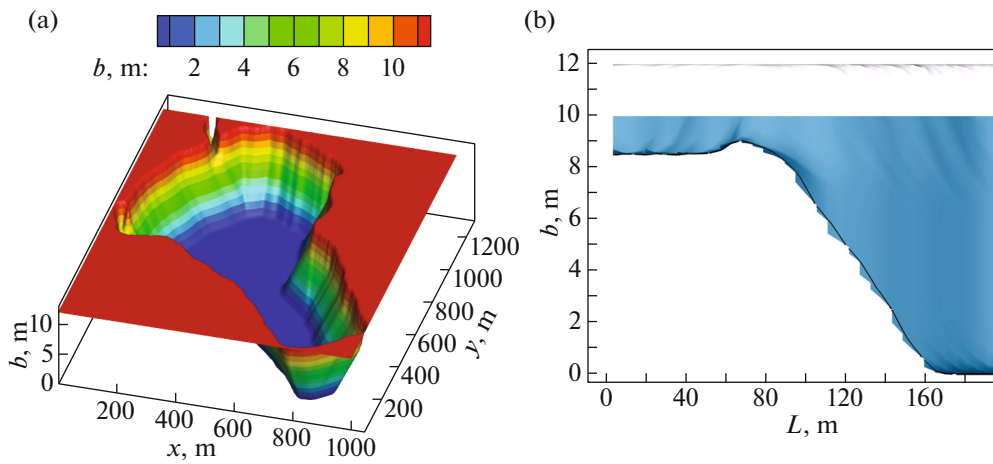

Fig. 18. (a) Model of the lake bathymetry and (b) the entrance of the channel to the lake (lengthwise section); L is the distance along the axis of the channel, and the water level is shown in blue ($\xi = 10$ m).

this process relies on a transport equation in which the inflowing low-temperature water is treated as a tracer. In this case, the tracer concentration can be assigned to the thickness of ice forming in the lake in the cold season, which is found to be thicker near the channel outlet than in the rest of the lake. Accordingly, in what follows, the concentration C is indicated in abstract dimensionless units.

For a physically correct simulation of the lake, as a body force, we added the Coriolis force

$$f_x = f^c u_y, \quad f_y = -f^c u_x.$$

For the entire domain, the Coriolis parameter $f^c = 2\Omega \sin \phi$, where $\Omega = 7.2921 \times 10^{-5}$ s^{-1} is the Earth's angular velocity, was set to the constant corresponding to the geographic latitude $\phi = 77.866667°$.

The following model was constructed for the bathymetry of the lake (see Fig. 18a). The water in the channel is 1 m deep, but there is a bump at the channel entrance to the lake, i.e., at the channel outlet (Fig. 18b). The channel is 10−12 m wide and about 200 m long. The depth of the lake is 10 m, and the height of the lake beach is 2 m.
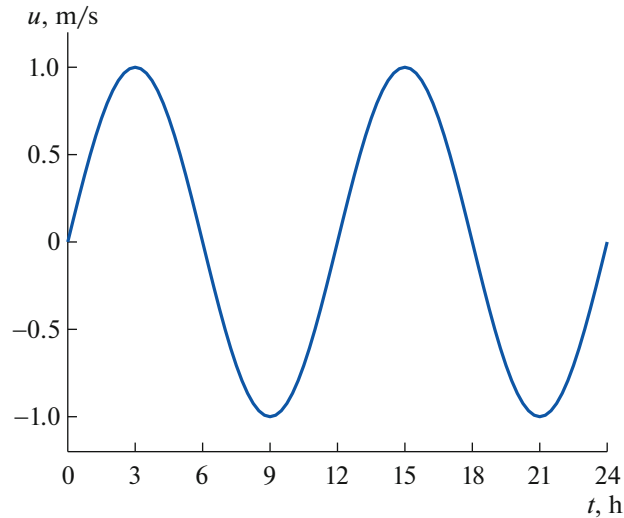
Fig. 19. Velocity $u_n = -u_y$ at the entrance to the lake.

Since the y axis is aligned with the normal to the boundary of the computational domain, for the simulation of the inflow of cold water into the lake, the boundary conditions at the channel outlet ($y = 1300$, Fig. 18a) were specified as

$$\frac{\partial h}{\partial y} = 0, \quad u_y = -\sin\left(\frac{\pi t}{6}\right) \text{m/s}, \quad u_x = 0 \text{ m/s}, \quad C = 1,$$

where the time t is indicated in hours. The profile of the normal velocity at the channel boundary is shown in Fig. 19.

The dry-bed condition (29), (30) was set on the other boundaries.

Since the diffusion coefficient of the tracer, i.e., in this case, the water thermal diffusivity D is very low ($D \sim 13.2 \times 10^{-8}$ m²/s at 0°C), in addition to the Navier–Stokes regularizer (11) in Eq. (10), the coefficient D in (13) was supplemented with an artificial term $\delta\mu$, where δ is a dimensionless coefficient determined by the numerical stability and accuracy requirements and μ is the viscosity taken from (11):

$$D \rightarrow D + \delta\mu, \quad \mu = \tau g h.$$

The need for this addition in the given problem is caused by the low velocity values; as a result, the dissipative term $\sim \tau h u^2$ in (13) becomes small.

In the computations discussed below, the numerical parameters were specified as

$$N_x = 247, \quad \Delta x \simeq 4.1 \text{ m},$$
$$N_y = 234, \quad \Delta y \simeq 5.4 \text{ m},$$
$$\alpha = 0.3, \quad \beta = 0.2, \quad \delta = 0.1, \quad \varepsilon = 0.01.$$

Figure 20 shows the flow pattern and level lines of the velocity magnitude $|u| = \sqrt{u_x^2 + u_y^2}$ at $t = 3$ h and $t = 9$ h, which correspond to the maximum and the minimum inflow rates. The velocity magnitude distribution (several centimeters per second away from the channel) agrees with the experimental observations of [16]. We can clearly see the formation of a circular vortex of diameter of 200–300 m, which also agrees with the experimental observations.

Figure 21 presents the tracer concentration distribution at $t = 3$ h and $t = 15$ h, which correspond to two maxima of the inflow rates. The concentration of the inflowing cold water determines the formation of ice and its thickness distribution as the lake freezes.

Overall, the solution exhibits a vortex structure; moreover, numerical experiments showed that the Coriolis force does not influence the circulation pattern, i.e., the circulation is determined only by the shape of the lake and the position of the inflow.
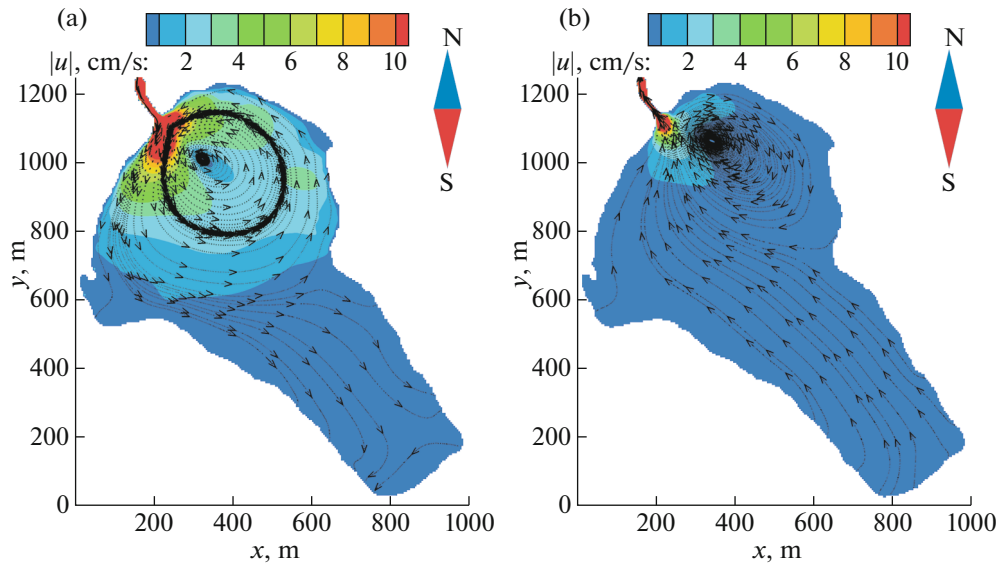
Fig. 20. Circulation in the lake and level lines of the velocity magnitude $|u|$ at (a) $t = 3$ h and (b) $t = 9$ h.
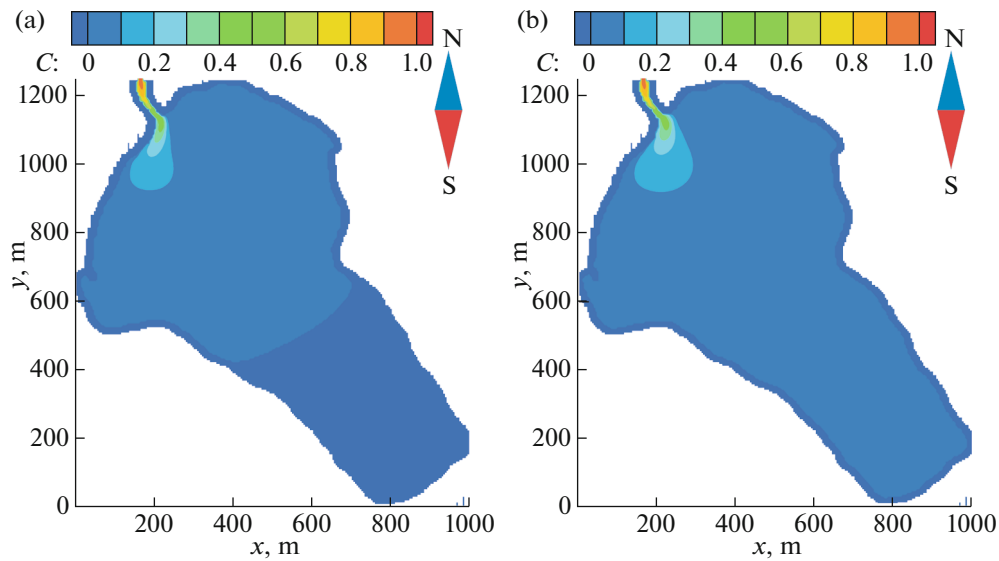

Fig. 21. Tracer concentration distribution in the lake at (a) $t = 3$ h and (b) $t = 15$ h.

Cold water concentrates near the channel outlet and, according to long-term observations [15, 16], this result agrees with the actual ice thickness distribution: the ice is much thicker in the vortex formation region.

7. CONCLUDING REMARKS

For the first time, we have constructed regularized hydrodynamic equations, together with the transport equation for a passive scalar, which can be regarded, for example, as the pollutant concentration in the fluid. In numerical experiments with shallow water flows, it was shown that the additional regularization for the passive scalar transport equation substantially improves the stability of its numerical solution as compared with the use of regularization only for the continuity and momentum equations.

A similar technique can be applied to the Navier−Stokes equations for nonisothermal viscous incompressible flows with the heat equation treated as a passive scalar transport equation with concentration C. In this case, the regularized system is written as

$$\nabla \cdot (\mathbf{u} - \mathbf{w}) = 0, \tag{39}$$

$$\frac{\partial \mathbf{u}}{\partial t} + \nabla \cdot ((\mathbf{u} - \mathbf{w}) \otimes \mathbf{u}) - \nu((\nabla \otimes \mathbf{u}) + (\nabla \otimes \mathbf{u})^{\mathrm{T}}) - \nabla \cdot (\mathbf{u} \otimes \mathbf{w}) = -\frac{1}{\rho_0}\nabla p + \mathbf{f}, \tag{40}$$

where the velocity is given by

$$\mathbf{w} = \tau((\mathbf{u} \cdot \nabla)\mathbf{u} + \frac{1}{\rho_0}\nabla p - \mathbf{f}), \tag{41}$$

and the regularized pollutant transport equation is

$$\frac{\partial C}{\partial t} + \nabla \cdot ((\mathbf{u} - \mathbf{w})C) = \nabla \cdot \left(\frac{\nu}{Sc}\nabla C + \tau\mathbf{u}(\nabla \cdot \mathbf{u}C)\right). \tag{42}$$

Here, $\frac{\nu}{Sc}$ is the diffusion coefficient of the pollutant or the thermal diffusivity in the case of a heat-conducting fluid.

Previously, an equation of form (42) was used without a term involving the gradient of C on the right-hand side, which led to significant oscillations of the numerical solution in the simulation of flows with high flow velocities.

ACKNOWLEDGMENTS

REFERENCES

1. A. Chertock, A. Kurganov, and G. Petrova, "Finite-volume-particle methods for models of transport of pollutant in shallow water," J. Sci. Comput. **27**, 189−199 (2006).

2. A. Chertock and A. Kurganov, "On a hybrid finite-volume-particle method," ESAIM: M2AN **38** (6), 1071−1091 (2004).

3. V. I. Kvon, D. V. Kvon, S. D. Zonov, et al., "Numerical calculation of flows and long-range transport of contaminants in lowland river reservoirs," J. Appl. Mech. Tech. Phys. **44** (6), 880−884 (2003).

4. A. I. Delis and T. Katsaounis, "A generalized relaxation method for transport and diffusion of pollutant models in shallow water," Comput. Methods Appl. Math. **4** (4), 410−430 (2004).

5. F. Benkhaldoun, I. Elmahi, and M. Seaid, "Well-balanced finite volume schemes for pollutant transport on unstructured meshes," J. Comput. Phys. **226**, 180−203 (2007).

6. E. M. Chaabelasri, I. Elmah, R. Abdellaoui, et al., "Well balanced adaptive simulation of pollutant transport by shallow water flows: Application to the Bay of Tangier," Int. J. Hydraulic Eng. **3** (1), 10−23 (2014).

7. M.-O. Bristeau and B. Perthame, "Transport of pollutant in shallow water using kinetic schemes," ESAIM: Proc. **10**, 9−21 (2001).

8. E. Audusse and M.-O. Bristeau, "Transport of pollutant in shallow water: A two time steps kinetic method," ESAIM: M2AN 37 (2), 389−416 (2003).

9. E. D. Fernandez-Nieto and G. Narbona-Reina, "Extension of WAF type methods to nonhomogeneous shallow water equations with pollutant," J. Sci. Comput. **36**, 193−217 (2008).

10. V. V. Churuksaeva and M. D. Mikhailov, "Numerical modeling of the fluid flow over the bottom topography," Vestn. Tom. Gos. Univ. Mat. Mekh. **27** (1), 51−60 (2014).

11. E. M. Chaabelasri, I. Elmah, R. Abdellaoui, et al., "Numerical solution of advection diffusion reaction equation coupled with shallow water equation," Int. J. Sci. Eng. Res. **8**, 256−262 (2017).

12. B. N. Chetverushkin, *Kinetic Schemes and Quasi-Gasdynamic System of Equations* (MAKS, Moscow, 2004; CIMNE, Barcelona, 2008).

13. Yu. V. Sheretov, *Continuum Dynamics under Spatiotemporal Averaging* (Izhevsk, Moscow) [in Russian].

14. T. G. Elizarova, *Quasi-Gas Dynamic Equations* (Nauchnyi Mir, Moscow, 2007; Springer, Berlin, 2009).

15. A. V. Marchenko and E. G. Morozov, "Asymmetric tide in Lake Vallunden (Spitsbergen)," Nonlinear Process Geophys. Discuss **20**, 935−944 (2013).
https://doi.org/10.5194/npg-20-935-2013

16. E. G. Morozov, A. V. Marchenko, K. V. Filchuk, et al., "Sea Ice evolution and internal wave generation due to a tidal jet in a frozen sea," Appl. Ocean Res. **87**, 179−191 (2019).
https://doi.org/10.1016/j.apor.2019.03.024

17. O. V. Bulatov and T. G. Elizarova, "Regularized shallow water equations and an efficient method for numerical simulation of shallow water flows," Comput. Math. Math. Phys. **51** (1), 160−174 (2011).

18. Yu. V. Sheretov, *Regularized Hydrodynamic Equations* (Tver. Gos. Univ., Tver', 2016) [in Russian].

19. T. G. Elizarova and A. V. Ivanov, Preprint No. 27, IPM RAN (Keldysh Inst. of Applied Mathematics, Russian Academy of Sciences, Moscow, 2019).

20. O. V. Bulatov and T. G. Elizarova, "Regularized shallow water equations for numerical simulation of flows with a moving shoreline," Comput. Math. Math. Phys. **56** (4), 661−679 (2016).

21. A. A. Zlotnik, "On construction of quasi-gasdynamic systems of equations and the barotropic system with the potential body force," Mat. Model. **24** (4), 65−79 (2012).

Translated by I. Ruzanova